Coordinated control strategies for active steering, differential braking and active suspension for vehicle stability, handling and safety improvement

Hussein Termous, Hassan Shraïm, Reine Talj, Clovis Francis, Ali Charara

Coordinated Control Strategies for Active Steering, Differential braking and Active Suspension for Vehicle Stability, Handling and Safety Improvement

Hussein Termous[1, 2], Hassan Shraim[1], Reine Talj[2], Clovis Francis[1], Ali Charara[2]

Abstract— **In this paper, a coordinated control strategy is proposed to provide an effective improvement in handling stability of the vehicle, safety and comfort riding for passengers. This control strategy is based on the coordination among active steering, differential braking, and active suspension systems. Two families of controllers are used for this purpose, which are the high order sliding mode and the backstepping controllers. The control strategy was tested on a full nonlinear vehicle model in the environment of MATLAB/Simulink. Rollover avoidance and yaw stability control constraints, have been considered. The control system mainly focuses on yaw stability control. When rollover risk is detected, the proposed strategy controls the roll dynamics to decrease rollover propensity. Simulation results for two different critical driving scenarios, the first one is a double lane change and the other one is a J-turn maneuver, show the effectiveness of the coordination strategy in stabilizing the vehicle, enhancing handling and reducing rollover propensity.**

Index Terms— **Active steering, active suspension, direct yaw control, backstepping control, Global Chassis Control (GCC), rollover, safety, sliding mode, vehicle dynamics, vehicle stability.**

I. Introduction

The increasing demand on highly comfort and safe automotive vehicles motivated industrials to integrate new control devices and techniques in their vehicles. Since developing precise control techniques depends on the model's accuracy, several studies have investigated vehicle models, starting from simplified models reaching highly nonlinear ones.

Global chassis control is an object of interest nowadays. Several active safety systems and actuators are introduced on modern vehicles to improve stability, handling and comfort, such as the active suspension system, active steering and active braking system. To increase ride comfort and vehicle road holding, many researchers applied various control methods on active suspension system, such as sliding mode controller [1], backstepping controller [2], LPV/H∞ control [3], fuzzy control [4], PID State Feedback Controller [5], and PID [6]. Few other papers develop controllers for the active suspension system for rollover prevention [7][8][9]. For longitudinal and lateral dynamics, research efforts have been focused on vehicle lateral stability by integrating active steering and differential braking system [10][11][12][13]. In this paper, a Global Chassis Control (GCC) has been proposed, based on a coordination control strategy between active suspension, active front steering and differential braking systems to ensure stability and rollover prevention on road vehicles.

Under critical driving circumstances, it is difficult for a driver to stabilize the vehicle, and dangerous accidents could happen. Safety of ground vehicles requires the improvement of yaw stability by active controllers (i.e. active steering and differential braking). Here, the basic idea is to assist the vehicle handling to be close to a linear vehicle handling characteristic that is familiar to the driver, and to restrain the vehicle lateral dynamics to be within the stable handling region in aggressive manoeuvres [14] .

By applying additional steering angle to the front wheels, Active Front Steering control (AFS) can enhance the steerability and thus lateral vehicle behavior by directly regulating yaw rate dynamics, through the lateral tire forces [15]. Unfortunately, AFS becomes less effective when the vehicle reaches the handling limits due to the tire forces saturations. In order to maintain the vehicle's stability under critical driving conditions, an alternative approach utilizes differential braking forces between the left and the right sides of the vehicle to produce the required corrective yaw moment [15]. This braking based technique is referred to as a Direct Yaw moment Control (DYC). Note that DYC is effective in both vehicle linear/nonlinear regions; however, it is not desirable in normal operation conditions because of the direct influence of the control action on the longitudinal vehicle dynamics (i.e. it causes the vehicle to slow down significantly).

Moreover, *Rollover* is one of the main forms in vehicle's traffic accident. In recent years rollover has become an important safety issue for a large class of vehicles. Even though rollovers constitute a small percentage of all accidents, they have a large contribution to severe and fatal injuries. Rollover is the primary cause of fatalities in accidents involving sport utility vehicles (SUVs)[16]. So, there is an urgent need to develop both analytical and experimental tools to predict rollover propensity of vehicles and to improve their design with respect to rollover prevention. Among the intelligent safety technologies for ground vehicles, active suspensions controlled by embedded computing elements for preventing rollover have received a lot of attention.

The existing models for synthesizing and allocating forces in such suspensions are conservatively based on the constraint that no wheels lift off the ground. The suspension systems play a key role in vehicle dynamics. Indeed, a well-designed suspension system may considerably improve not only the passenger comfort, but also the car road holding. Several control design problems for suspension systems have then been tackled with many approaches during the last decades.

For ride comfort, it is necessary to reduce the vertical, pitch and roll accelerations. However, this does not guarantee rollover prevention.

1: Lebanese University, Faculty of Engineering, Scientific research Center in Engineering (CRSI), Campus Rafic Hariri, Beirut, Lebanon, Email: husseintermous@gmail.com; {cfrancis, hassan.shraim}@ul.edu.lb.

2: Sorbonne Universités, Université de Technologie de Compiègne, CNRS, UMR 7253 Heudiasyc, 60200 Compiègne, France, Email:
{ ali.charara,reine.talj}@hds.utc.fr;

Generally, it is desirable to reduce the roll angle or roll rate to prevent rollover.

In this work, the design of a global vehicle control scheme that integrates and coordinates braking, front steering, and active suspension systems is presented to enhance vehicle handling, yaw stability, safety and comfort. This paper is organized as follows: Section 2 expresses the four-wheel full vehicle model. Section 3 describes the vehicle reference model (bicycle model) that will be used to generate the desired reference variables that the vehicle dynamics must follow. Section 4 introduces the actuators model used for the three active systems. Section 5 describes the Active Front Steering (AFS) controller, the Direct Yaw moment Controller (DYC) and the Active Suspension controller (AS) that were designed as stand-alone controllers using two robust approaches, a high order super-twisting sliding mode control and backstepping control. Section 6 shows in details the proposed coordinated control strategy. Section 7 shows the simulation results for two different critical driving scenarios, the first one shows the effectiveness of the coordination strategy in stabilizing the vehicle and enhancing handling. The second scenario shows the effectiveness of the coordination strategy in reducing rollover propensity.

NOMENCLATURE

Symbol	*Physical Meaning*
$\boldsymbol{CoG}$	Center of Gravity
$\boldsymbol{z}$	Vertical displacement of CoG
$\boldsymbol{z_s}$	Vertical displacement of the corner
$\boldsymbol{z_u}$	Vertical displacement of the wheel
$\boldsymbol{z_r}$	Road perturbation
$\boldsymbol{\theta}$	Pitch angle
$\boldsymbol{\phi}$	Roll angle
$\dot{\boldsymbol{\phi}}$	Roll rate
$\boldsymbol{\psi}$	Yaw angle
$\dot{\boldsymbol{\psi}}$	Yaw rate
$\boldsymbol{a_x}$	Longitudinal acceleration
$\boldsymbol{a_y}$	Lateral acceleration
$\boldsymbol{F_x}$	Wheel longitudinal force
$\boldsymbol{F_y}$	Wheel Lateral force
$\boldsymbol{F_z}$	Tire-ground contact force
$\boldsymbol{\delta}$	Driver steering angle
$\boldsymbol{\Omega}$	Angular velocity of the wheel
$\boldsymbol{v_x}$	Longitudinal speed of the wheel
$\boldsymbol{\beta}$	Vehicle side-slip angle
$\dot{\boldsymbol{x}}$	Vehicle longitudinal speed
$\dot{\boldsymbol{y}}$	Vehicle lateral speed
$\boldsymbol{\alpha}$	Wheel slip angle
$\boldsymbol{\sigma_x}$	Wheel longitudinal slipping
$\boldsymbol{C_m}$	Motor torque applied on the wheel
$\boldsymbol{C_b}$	Braking torque applied on the wheel
$\boldsymbol{\mu}$	Coefficient of adherence
$\boldsymbol{f}$	Active suspension force

Table I

SIMULATION PARAMETERS

Parameter	*Value*	*Unit*	*Physical Meaning*
$\boldsymbol{M}$	1465	kg	Total mass of Vehicle
$\boldsymbol{m_s}$	1286	kg	Sprung mass of the vehicle
$\boldsymbol{m_u}$	40	kg	Unsprung mass
$\boldsymbol{I_z}$	1972	$kg.m^2$	Moment of inertia around the yaw axis
$\boldsymbol{I_x}$	535	$kg.m^2$	Moment of inertia around the x - axis
$\boldsymbol{I_y}$	1859	$kg.m^2$	Moment of inertia around the y - axis
$\boldsymbol{I_r}$	1	$kg.m^2$	Moment of inertia around wheel axis
$\boldsymbol{a}$	1	m	Distance from front axle to CoG
$\boldsymbol{b}$	1.6	m	Distance from rear axle to CoG
$\boldsymbol{w}$	0.773	m	Half Vehicle widths axle
$\boldsymbol{k_{s,f}}$	12548	N/m	Front suspension stiffness coefficient
$\boldsymbol{k_{s,r}}$	22639	N/m	Rear suspension stiffness coefficient
$\boldsymbol{c_{s,f}}$	1500	Ns/m	Front suspension damping coefficient
$\boldsymbol{c_{s,r}}$	3000	Ns/m	Rear suspension damping coefficient
$\boldsymbol{k_{t,f}}$	473520	N/m	Front wheel stiffness coefficient
$\boldsymbol{k_{t,r}}$	460780	N/m	Rear wheel stiffness coefficient
$\boldsymbol{c_t}$	100	Ns/m	Wheel damping coefficient
$\boldsymbol{h}$	0.52	m	CoG height
$\boldsymbol{h_r}$	0.4	m	Distance from pitch axle to CoG
$\boldsymbol{h_u}$	0.4	m	Distance from roll axle to CoG
$\boldsymbol{r}$	0.308	m	Wheel radius
$\boldsymbol{C_\sigma}$	18700	N/rad	Longitudinal stiffness of the tire
$\boldsymbol{C_\alpha}$	76776	N/rad	Lateral stiffness of the tire

Table II

II. FULL VEHICLE MODEL

Vehicle models have been widely studied in the literature, starting from simplified models or bicycle models to highly complex models [17][18][19][20][1]. In this section, we present the full vehicle model taking into consideration most of the nonlinearities existing in the vehicle dynamics. The proposed model is composed of several subsystems: Vertical Dynamics, Lateral and longitudinal Dynamics, Wheel Dynamics, Wheel-ground contact forces.

A. Vertical Dynamics

By the vertical dynamics, we mean the vertical displacement of the center of gravity (CoG), z, rotation of the system around x-axis, the

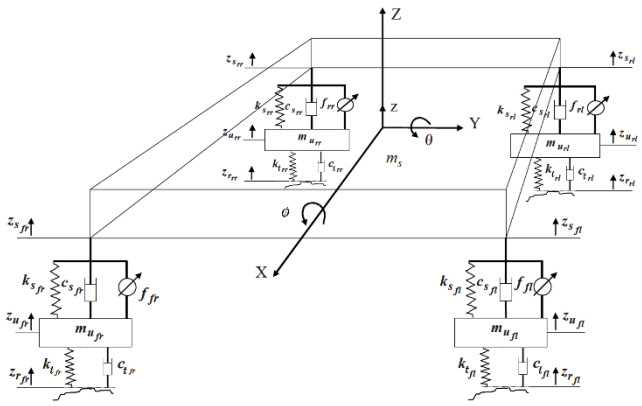

Figure 1. Full vertical model.

roll angle ϕ, and rotation around y-axis, the pitch angle θ.

Using Newton's laws, dynamics of the suspended mass (chassis) are as follows:

$$\begin{cases} \ddot{z} = f_z(x,\dot{x}) + g_z(x,\dot{x})u_z \\ \ddot{\theta} = f_\theta(x,\dot{x}) + g_\theta(x,\dot{x})u_\theta \\ \ddot{\phi} = f_\phi(x,\dot{x}) + g_\phi(x,\dot{x})u_\phi \end{cases} \quad (1)$$

Where:

$$\begin{aligned} M * \boldsymbol{f_z}(\boldsymbol{x},\dot{\boldsymbol{x}}) = \{ & k_{s_{fr}} z_{u_{fr}} + k_{s_{fl}} z_{u_{fl}} + k_{s_{rr}} z_{u_{rr}} + k_{s_{rl}} z_{u_{rl}} + (k_{s_{fr}} + k_{s_{fl}} + k_{s_{rr}} + k_{s_{rl}})z - [a(k_{s_{fr}} + k_{s_{fl}}) - b(k_{s_{rr}} + k_{s_{rl}})]sin\theta - [w(k_{s_{fl}} + k_{s_{rl}}) - w(k_{s_{fr}} + k_{s_{rr}})]sin\phi + c_{s_{fr}}\dot{z}_{u_{fr}} + c_{s_{fl}}\dot{z}_{u_{fl}} + c_{s_{rr}}\dot{z}_{u_{rr}} + c_{s_{rl}}\dot{z}_{u_{rl}} - (c_{s_{fr}} + c_{s_{fl}} + c_{s_{rr}} + c_{s_{rl}})\dot{z} - [a(c_{s_{fr}} + c_{s_{fl}}) - b(c_{s_{rr}} + c_{s_{rl}})]cos\theta\dot{\theta} - [w(c_{s_{fl}} + c_{s_{rl}}) - w(c_{s_{fr}} + c_{s_{rr}})]cos\phi\dot{\phi}\} \end{aligned} \quad (2)$$

$$\begin{aligned} I_y * \boldsymbol{f_\theta}(\boldsymbol{x},\dot{\boldsymbol{x}}) = cos\theta\{ & ak_{s_{fr}} z_{u_{fr}} + ak_{s_{fl}} z_{u_{fl}} - bk_{s_{rr}} z_{u_{rr}} - bk_{s_{rl}} z_{u_{rl}} - [a(k_{s_{fr}} + k_{s_{fl}}) - b(k_{s_{rr}} + k_{s_{rl}})]z - [a^2(k_{s_{fr}} + k_{s_{fl}}) + b^2(k_{s_{rr}} + k_{s_{rl}})]sin\theta - [w(ak_{s_{fl}} - bk_{s_{rl}}) - w(ak_{s_{fr}} - bk_{s_{rr}})]sin\phi + ac_{s_{fr}}\dot{z}_{u_{fr}} + ac_{s_{fl}}\dot{z}_{u_{fl}} - bc_{s_{rr}}\dot{z}_{u_{rr}} - bc_{s_{rl}}\dot{z}_{u_{rl}} - [a(c_{s_{fr}} + c_{s_{fl}}) - b(c_{s_{rr}} + c_{s_{rl}})]\dot{z} - [a^2(c_{s_{fr}} + c_{s_{fl}}) + b^2(c_{s_{rr}} + c_{s_{rl}})]cos\theta\dot{\theta} - [w(ac_{s_{fl}} - bc_{s_{rl}}) - w(ac_{s_{fr}} - bc_{s_{rr}})]cos\phi\dot{\phi} - m_s.h_r.a_x\} \end{aligned} \quad (3)$$

$$\begin{aligned} I_x * \boldsymbol{f_\phi}(\boldsymbol{x},\dot{\boldsymbol{x}}) = cos\phi\{ & -wk_{s_{fr}} z_{u_{fr}} + wk_{s_{fl}} z_{u_{fl}} - wk_{s_{rr}} z_{u_{rr}} + wk_{s_{rl}} z_{u_{rl}} - [w(k_{s_{fl}} + k_{s_{rl}}) - w(k_{s_{fr}} + k_{s_{rr}})]z - [w^2(k_{s_{fl}} + k_{s_{rl}}) + w^2(k_{s_{fr}} + k_{s_{rr}})]sin\phi - [w(ak_{s_{fl}} - bk_{s_{rl}}) - w(ak_{s_{fr}} - bk_{s_{rr}})]sin\theta - wc_{s_{fr}}\dot{z}_{u_{fr}} + wc_{s_{fr}}\dot{z}_{u_{fr}} - wc_{s_{fr}}\dot{z}_{u_{fr}} + wc_{s_{fr}}\dot{z}_{u_{fr}} - [w(c_{s_{fl}} + c_{s_{rl}}) - w(c_{s_{fr}} + c_{s_{rr}})]\dot{z} - [w^2(c_{s_{fl}} + c_{s_{rl}}) + w^2(c_{s_{fr}} + c_{s_{rr}})]cos\phi\dot{\phi} - [w(ac_{s_{fl}} - bc_{s_{rl}}) - w(ac_{s_{fr}} - bc_{s_{rr}})]cos\theta\dot{\theta} + m_s.h_u.a_y\} \end{aligned} \quad (4)$$

$$\begin{cases} g_z(x,\dot{x}) = 1/M \\ g_\theta(x,\dot{x}) = cos\theta/I_y \\ g_\phi(x,\dot{x}) = cos\phi/I_x \end{cases} \quad (5)$$

$$\begin{cases} u_z = f_{fr} + f_{fl} + f_{rr} + f_{rl} \\ u_\theta = a(f_{fr} + f_{fl}) - b(f_{rr} + f_{rl}) \\ u_\phi = -w(f_{fr} + f_{rr}) + w(f_{fl} + f_{rl}) \end{cases} \quad (6)$$

Where the dynamics of the non-suspended mass is as the following:

$$\ddot{z}_{u_\vartheta} = [k_{s_\vartheta}(z_{s_\vartheta} - z_{u_\vartheta}) + c_{s_\vartheta}(\dot{z}_{s_\vartheta} - \dot{z}_{u_\vartheta}) + k_{t_\vartheta}(z_{r_\vartheta} - z_{u_\vartheta}) + c_{t_\vartheta}(\dot{z}_{r_\vartheta} - \dot{z}_{u_\vartheta}) - f_\vartheta]/m_\vartheta \quad (7)$$

With $\vartheta = \{fr, fl, rr, rl\}$

and the displacements on each corner of the chassis are:

$$\begin{aligned} z_{s_{fr}} &= z - wsin\phi + asin\theta \\ z_{s_{fl}} &= z + wsin\phi + asin\theta \\ z_{s_{rr}} &= z - wsin\phi - bsin\theta \\ z_{s_{rl}} &= z + wsin\phi - bsin\theta \end{aligned} \quad (8)$$

B. Lateral and longitudinal Dynamics

In this section, we use the Four-wheel vehicle model (FWVM), commonly called the two tracks model, and widely used in the literature to study and control the longitudinal and transversal vehicle dynamics behavior [21], [22]. This model has the advantage that it clearly represents the four wheels. Fig. 2 shows plane scheme for the vehicle.

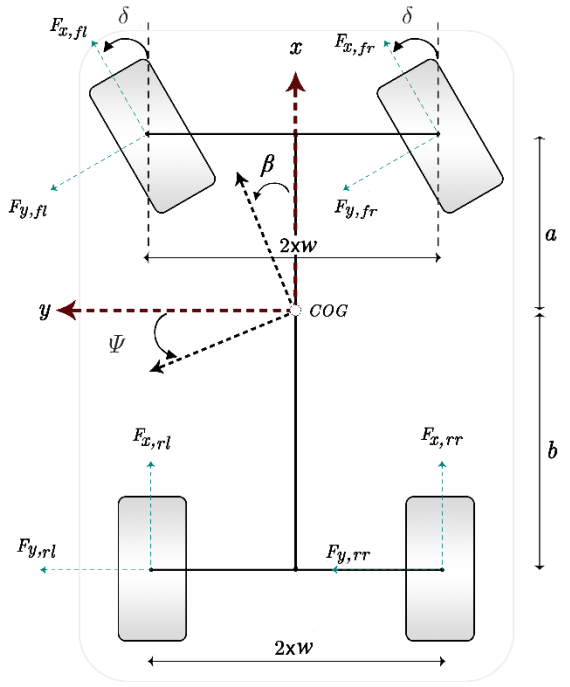

Figure 2. 2D representation of a four-wheel vehicle model.

Applying Newton's second law to the lumped vehicle mass longitudinally, laterally and about a vertical axis through the center of mass produces the following equations of motion:

$$M\ddot{x} = M\dot{\psi}\dot{y} - F_{x,res} + cos\delta(F_{x,fr} + F_{x,fl}) + F_{x,rr} + F_{x,rl} - sin\delta(F_{y,fr} + F_{y,fl}) \quad (9)$$

$$M\ddot{y} = -M\dot{\psi}\dot{x} - F_{y,res} + sin\delta(F_{x,fr} + F_{x,fl}) + F_{y,rr} + F_{y,rl} + cos\delta(F_{y,fr} + F_{y,fl}) \quad (10)$$

$$I_z\ddot{\psi} = M_{res} - w(cos\delta(F_{x,fl} - F_{x,fr}) + sin\delta(F_{y,fr} - F_{y,fl})) + a(sin\delta(F_{x,fl} + F_{x,fr}) + cos\delta(F_{y,fl} + F_{y,fr})) - b(F_{y,rr} + F_{y,rl}) - w(F_{x,rl} - F_{x,rr}) \quad (11)$$

$$a_y = \ddot{y} + \dot{x}\dot{\psi} \quad (12)$$

$$a_x = \ddot{x} - \dot{y}\dot{\psi} \quad (13)$$

$$\beta = arctan(\dot{y}/\dot{x}) \quad (14)$$

Knowing that $\ddot{x}$ *and* $\ddot{y}$ are the longitudinal and lateral acceleration in the mobile frame reference of the vehicle. Where a_y *and* a_x are the longitudinal and lateral acceleration in the fixed frame reference.

C. *Wheels Dynamics*

The four equations describing the angular velocity of each wheel are:

$$I_r\dot{\Omega}_\vartheta = -r_\vartheta F_{x,\vartheta} + C_{m,\vartheta} - C_{b,\vartheta} \quad (15)$$

Each wheel has its longitudinal speed, which can be found by applying the classical principles of physics and are given by the following formulas:

$$v_{x,fr} = (\dot{x} + c\dot{\psi})cos\delta + (\dot{y} + a\dot{\psi})sin\delta \quad (16)$$
$$v_{x,fl} = (\dot{x} - c\dot{\psi})cos\delta + (\dot{y} + a\dot{\psi})sin\delta \quad (17)$$
$$v_{x,rr} = \dot{x} + w\dot{\psi} \quad (18)$$
$$v_{x,rl} = \dot{x} - w\dot{\psi} \quad (19)$$

Due to the elasticity of the tire and under the effect of the transversal efforts, a torque of auto alignment is created, this torque modifies the initial direction of the wheel by an angle called slip angle. So the slip angle can be defined as the angle that exists between the velocity vector of the wheel and the orientation of the wheel, it is calculated in the following way:

$$\begin{aligned} \alpha_{fr} &= \delta - arctan\left(\frac{\dot{y} + a\dot{\psi}}{\dot{x} + w\dot{\psi}}\right) \\ \alpha_{fl} &= \delta - arctan\left(\frac{\dot{y} + a\dot{\psi}}{\dot{x} - w\dot{\psi}}\right) \\ \alpha_{rr} &= -arctan\left(\frac{\dot{y} - b\dot{\psi}}{\dot{x} + w\dot{\psi}}\right) \\ \alpha_{rl} &= -arctan\left(\frac{\dot{y} - b\dot{\psi}}{\dot{x} - w\dot{\psi}}\right) \end{aligned} \quad (20)$$

The longitudinal slipping for each of the four wheels is given by the following equations:

$$\sigma_{x,\vartheta} = \begin{cases} \dfrac{r\Omega_\vartheta - v_{x,\vartheta}}{r\Omega_\vartheta} & during\ acceleration \\ \dfrac{r\Omega_\vartheta - v_{x,\vartheta}}{v_{x,\vartheta}} & during\ braking \end{cases} \quad (21)$$

The term slip expresses the difference between the wheel velocity and the vehicle velocity when a driving or braking force is applied on the tire [23].

D. *Wheel-ground contact forces*

The vertical load on each tire can be expressed by the following equations:

$$F_{z,\vartheta} = m_{z\vartheta} - k_{t_\vartheta}(z_{u_\vartheta} - z_{r_\vartheta}) - c_{t_\vartheta}(\dot{z}_{u_\vartheta} - \dot{z}_{r_\vartheta}) \quad (22)$$

The lateral and longitudinal contact forces on each tire can be expressed by the following equations based on the Dugoff's model [24]:

$$F_{x,\vartheta} = C_\sigma \frac{\sigma_{x,\vartheta}}{1 - \sigma_{x,\vartheta}} f(\lambda_\vartheta) \quad (23)$$

$$F_{y,\vartheta} = C_\alpha \frac{tan(\alpha_\vartheta)}{1 - \sigma_{x,\vartheta}} f(\lambda_\vartheta) \quad (24)$$

$$f(\lambda_\vartheta) = \begin{cases} (2 - \lambda_\vartheta)\lambda_\vartheta & for\ \lambda_\vartheta < 1 \\ 1 & for\ \lambda_\vartheta \geq 1 \end{cases} \quad (25)$$

$$\lambda_\vartheta = \frac{\mu F_{z_\vartheta}(1 - \sigma_{x,\vartheta})}{2\sqrt{(C_\alpha\,\sigma_{x,\vartheta})^2 + (C_\sigma tan(\alpha_\vartheta))^2}} \quad (26)$$

It provides a simple formulation and the ability to describe forces under pure cornering, pure acceleration/braking and combined acceleration (braking)/cornering maneuvers. It assumes a uniform vertical pressure distribution on the tire contact patch. Compared to the Magic formula tire model, Dugoff's model offers one significant advantage; it synthesizes all the tire property parameters into two constants, C_σ and C_α, called longitudinal and cornering (lateral) stiffness of the tires[21].

III. Reference Vehicle Model

The modeling of the vehicle movement can be considerably simplified by using a bicycle model of the vehicle. It is also known as the single track model. The bicycle model shown in Fig. 3 will be used to generate the dynamic reference which is desired by the driver without the existence of any external disturbances. For that the bicycle model is simplified to only account for the slip angle β_{ref} and the yaw rate $\dot{\psi}_{ref}$, representing the lateral dynamics of the vehicle in normal driving conditions.

This model is one of the most widely known models and it is fully described in [25]. The dynamic equations of the vehicle reference model can be written as follows:

$$\begin{cases} \dot{\beta}_{ref} = -\dot{\psi}_{ref} + \dfrac{1}{M\dot{x}}\left[C_f\left(\delta - \beta_{ref} - \dfrac{a\dot{\psi}_{ref}}{\dot{x}}\right) + C_r\left(-\beta_{ref} + \dfrac{b\dot{\psi}_{ref}}{\dot{x}}\right)\right] \\ \ddot{\psi}_{ref} = \dfrac{1}{I_z}\left[aC_f\left(\delta - \beta_{ref} - \dfrac{a\dot{\psi}_{ref}}{\dot{x}}\right) - bC_r\left(-\beta_{ref} + \dfrac{b\dot{\psi}_{ref}}{\dot{x}}\right)\right] \end{cases} \quad (27)$$

Where C_f *and* C_r are the rigidity of front and rear wheels axles respectively, and for reason of safety β_{ref} and $\dot{\psi}_{ref}$ must be limited as follows [26]:

$$|\dot{\psi}_{ref,max}| \leq \left|\frac{0.85\mu g}{\dot{x}}\right| \quad \& \quad \beta_{ref,max} = arctan(0.02\mu g) \quad (28)$$

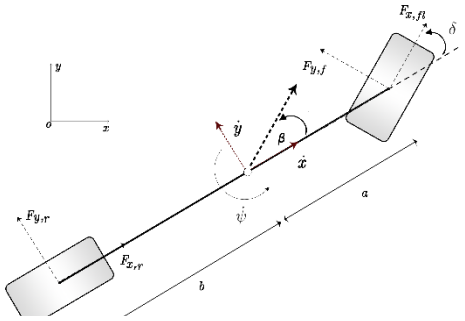

Figure 3. Bicycle model.

The standalone controllers AFS & DYC are synthesized based on the linear bicycle model, this relatively simple model represents the lateral vehicle dynamics. However, it should be slightly modified taking into account the controller's objectives and structure, the model is extended to include two control inputs from the active stability systems:

- The direct yaw moment M_Z^* that will be transformed into the corresponding differential rear braking torque of the DYC.
- The steering angle δ is written as the sum of the driver's steering input δ_d and the additive front steering input δ_c^* of the AFS.

Then the dynamic equations of the vehicle synthesis model will be written as follows:

$$\begin{cases} \dot{\beta} = -\dot{\psi} + \dfrac{1}{M\dot{x}}\left[\begin{matrix} C_f\left(\delta_d + \delta_c^* - \beta - \dfrac{a\dot{\psi}}{\dot{x}}\right) \\ +C_r\left(-\beta + \dfrac{b\dot{\psi}}{\dot{x}}\right)\end{matrix}\right] \\ \ddot{\psi} = \dfrac{1}{I_z}\left[\begin{matrix} aC_f\left(\delta_d + \delta_c^* - \beta - \dfrac{a\dot{\psi}}{\dot{x}}\right) \\ -bC_r\left(-\beta + \dfrac{b\dot{\psi}}{\dot{x}}\right) + M_Z^*\end{matrix}\right] \end{cases} \quad (29)$$

IV. Actuators Model

The actuators models for active steering and differential braking are added to the global control scheme to take into consideration their dynamic response with respect to the control input signals. The following models used in [11] will be adopted:

A. A steer-by-wire Active steering system that will generate an additive steering angle applied to the front wheel axle and modeled as:

$$\dot{\delta}_c = 2\pi f_1(\delta^+ - \delta_c) \quad (30)$$

Where $f_1 = 10Hz$ is the cut-off frequency, $\delta^+ \; and \; \delta_c$ are the output of the steering controller and actuator respectively. The output of the actuator is limited between [-5°, 5°].

B. A brake-by-wire electromechanical braking system that will provide the positive braking torque modeled as:

$$\dot{T}_{b_{rj}} = 2\pi f_2(\bar{T}_{b_{rj}} - T^*_{b_{rj}}) \quad (31)$$

Where $f_2 = 10Hz$ is the cut-off frequency, $\bar{T}_{b_{rj}} and \; T^*_{b_{rj}}$ are the output of the ABS rear local controller and the actuator respectively. The output of the actuator is limited between [0, 1200] N.m. The braking torque is only applied to the rear wheels to avoid any interference with the front active steering command.

ABS Control Strategy:

The Anti-lock Braking System (ABS) control strategy is reproduced and added to the global scheme at the rear wheels where the braking command is applied. This local controller is used to avoid slipping situations leading to loss of maneuverability. It achieves good braking performances. When the required braking control torque $T^d_{b_{rj}}$ is too high, it might lead to a skidding situation and an ABS strategy is needed. The principle of this ABS relies on the mixed slip / deceleration method developed in [27]

$$\bar{T}_{b_{rj}} = min(T^d_{b_{rj}}, T_{ABS,brj}) \quad (32)$$

If the braking torque $T^d_{b_{rj}}$ exceeds $T_{ABS,brj}$, the braking torque determined by the ABS, a skidding situation takes place and the ABS is activated.

C. Active Suspension System

The dynamics of the actuator of the active suspension system is represented by the following equation [1]:

$$\dot{A} = -\beta_a A - \kappa S(\dot{z}_S - \dot{z}_U) + sign(p_s - sign(z_v)A)\gamma\sqrt{|p_s - sign(z_v)A|}\, z_v \quad (33)$$

Where A represents the pressure given by the actuator, z_v the displacement of the servo valves, S is the area of the piston, p_s the provided pressure, $\dot{z}_S - \dot{z}_U$ the velocity of suspension deflection and β_a, $\kappa \; and \; \gamma$ are constant parameters.

The dynamics of the servo valves is represented by the following equation:

$$\dot{z}_v = \frac{1}{\tau}(-z_v + u) \quad (34)$$

Where τ is the time constant, u is the entered command such that $u = Ri$, i is the current of the coil of the servo-valve and R is the gain or resistance of servo-valve.

Four actuators are used, one at every corner of the vehicle providing the necessary force f_ϑ, such that $f_\vartheta = SA_\vartheta$.

V. Controllers

A. Active Steering controller

This controller aims to control the maneuverability of the vehicle by reducing the yaw rate error, by determining the additive steering angle δ_c^* that will be added to the driver's steering input at the front wheels. Let the corresponding sliding variable S_1 be:

$$S_1 = e_{\dot{\psi}} = \dot{\psi} - \dot{\psi}_{ref} \quad (35)$$

Where $\dot{\psi}$ and $\dot{\psi}_{ref}$ are obtained from the synthesis vehicle model and the vehicle reference model respectively. It can be easily seen from (29) that the control input δ_c^* appears explicitly in the first time derivative of S_1. Therefore, the system has a relative degree of one with respect to S_1. Hence, we can apply the second order Sliding Mode Control (SMC), super-twisting algorithm, where the control law acts on the time derivative of the sliding variable S_1 and guarantees $\dot{S}_1 = S_1 = 0$. The following expression must be derived for the corresponding sliding variable

$$\dot{S}_1 = \xi_1(t, S_1) + \varphi_1(t, S_1)\delta_c^* \quad (36)$$

On the other hand, we have:

$$\dot{S}_1 = \dot{e}_{\dot{\psi}} = \ddot{\psi} - \ddot{\psi}_{ref} \quad (37)$$

It is necessary to assume some conditions over ξ_1 and $\varphi_1$to guarantee the reachability of the sliding surface S_1=0 in finite time:

$$0 < k_1 < |\varphi_1| < K_1 \; and \; |\xi_1| < C_1 \tag{38}$$

For all $|S_1| < S_{1,0}$, where $k_1, K_1, C_1 \; and \; S_{1,0}$ are positive constants. There exist different kinds of second order SMC algorithms in the literature [28]. Generally, most of the second order sliding mode requires the measurement of S_1 and $\dot{S_1}$ to be available except the super-twisting algorithm where S_1 is the only needed variable. This algorithm has been developed to control systems with relative degree one and to avoid the chattering phenomena. The trajectories on the sliding plane $(S_1; \dot{S_1})$ are characterized by twisting around the origin. The control law $\delta_c^* = \delta_{c_1}^* + \delta_{c_2}^*$ is composed of two terms that do not depend on $\dot{S_1}$:

$$\begin{cases} \dot{\delta}_{c_1}^* = -\rho_1 sign(S_1) \\ \delta_{c_2}^* = -\alpha_1 |S_1|^{0.5} sign(S_1) \\ \rho_1, \alpha_1 > 0 \end{cases} \tag{39}$$

ρ_1 and α_1 should satisfy the sufficient conditions precised in [29] to guaranty the convergence in finite time on the sliding surface. The conditions over ρ_1 and α_1 are function of the sliding variable behavior, i.e. a function of the vehicle synthesis model, the reference model and the vehicle's parameters:

$$\rho_1 > \frac{C_1}{k_1} \; and \; \alpha_1 \geq \frac{4C_1(K_1 \rho_1 + C_1)}{{k_1}^2 (k_1 \rho_1 - C_1)} \tag{40}$$

B. Direct Yaw Controller

To guarantee the lateral stability of the vehicle, the objective of this controller is to reduce the vehicle's side-slip error and its time derivative by computing a corrective yaw moment M_z^* which will then be transformed into a braking torque $T_{b_r}^*$. The same methodology used in subsection *A* is used in this subsection, and the sliding variable S_2 which was used in [10]. S_2 is defined as:

$$S_2 = (\beta - \beta_{ref}) + \chi(\dot{\beta} - \dot{\beta}_{ref}) \quad with \; \chi > 0 \tag{41}$$

Where $\beta, \beta_{ref} \; and \; \dot{\beta}, \dot{\beta}_{ref}$ are obtained from the synthesis and reference vehicle models. It is simple to verify that the system has also a relative degree of one with respect to S_2 and the control input M_z^*. The super-twisting algorithm is then used to derive the control input M_z^* after deriving ξ_2 and φ_2. The control law is constituted of two terms $M_z^* = M_{z_1}^* + M_{z_2}^*$ with:

$$\begin{cases} \dot{M}_{z_1}^* = -\rho_2 sign(S_2) \\ M_{z_2}^* = -\alpha_2 |S_2|^{0.5} sign(S_2) \\ \rho_2, \alpha_2 > 0 \end{cases} \tag{42}$$

Same conditions over ρ_1 and α_1 described by (40) imply on ρ_2 and α_2.

The corrective yaw moment M_z^* can be generated by applying different braking forces on the two sides of the rear wheels axle or by braking only one wheel at a time. From an optimal point of view, it is recommended to brake only one wheel at a time [30]. Moreover, the vehicle is more decelerated when both wheels are braked to generate the same amount of M_z^* .

In [12] the equivalent torque difference $\Delta T^*_{b,r} = T^*_{b,rl} - T^*_{b,rr}$ between the left and right sides of the rear axle can be expressed in terms of M_z^* :

$$\Delta T_{b,r}^* = \frac{2M_z^* r}{w} \tag{43}$$

The brake torque applied to the wheel must be positive; therefore, the choice of the wheel to be controlled is done as following:

$$\begin{cases} if \; \Delta T_{b_r} < 0; \; T_{b_{rr}} = -\Delta T_{b_r}, \;\; T_{brl} = 0 \\ if \; \Delta T_{b_r} > 0; \; T_{b_{rl}} = \Delta T_{b_r}, \;\; T_{brr} = 0 \end{cases} \tag{44}$$

C. Active suspension Controller

In this section, the design of a two-level controller is proposed for active suspension system. The required control force f_ϑ is computed by applying a high-level controller, which is designed using a backstepping method. The suspension structure contains nonlinear components, i.e. the dynamics of the dampers, the springs and the actuator dynamics. The actuator generating the necessary control force is a nonlinear state dependent switching system, for which a low-level backstepping-based force-tracking controller is also designed. The two levels structure is illustrated in the following scheme (Fig. 4) where $z_{ref}, \theta_{ref} \; and \; \phi_{ref}$ are equal to zero in our study, seeking the objective of providing comfort for passenger and road holding.

We assume that the reference for f_ϑ (which is a linear function of A_ϑ) is given by the high-level controller. The goal is to asymptotically track

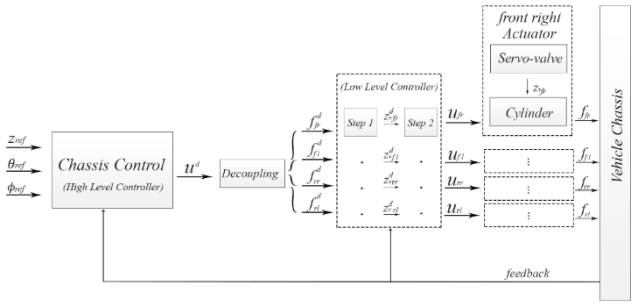

Figure 4. Structure of two level controller.

this reference with the actuator dynamics.

a. Low-Level controller (Active suspension Actuator)

The objective of this controller is to track the forces provided by the high-level controller f_ϑ^d . This controller takes as input the desired forces and gives the needed control inputs u_ϑ as shown in Figure 4. The backstepping design for the actuator subsystem can be performed in two steps. The reference computed by the high level controller is denoted by f^d, then $A^d = f^d/S$.

The pressure error can be expressed by the following equation:

$$e_A = A - A^d \tag{45}$$

In order to ensure that the pressure error converges to zero, it is sufficient that the required tracking error dynamics be defined as:

$$\begin{aligned} \dot{e}_A &= -\eta_1 e_A \\ \dot{A} - \dot{A^d} &= -\eta_1 (A - A^d) \; with \; \eta_1 > 0 \end{aligned} \tag{46}$$

let $Q = sign(p_s - sign(z_v)A)\gamma\sqrt{|p_s - sign(z_v)A|}$, then (46) can be

written as follows:

$$z_v Q = \beta_a A + \kappa S(\dot{z}_S - \dot{z}_u) + \dot{A^d} - \eta_1(A - A^d) \quad (47)$$

Then the reference for z_v is given by:

$$z_v{}^d = \frac{\beta_a A + \kappa S(\dot{z}_S - \dot{z}_u) + \dot{A^d} - k_1(A - A^d)}{Q} \quad (48)$$

The second step is to choose a control input u that converges the error $e_{z_v} = z_v - z_v{}^d$ to zero. Then to ensure the convergence, the tracking error dynamics is chosen as:

$$\dot{e}_{z_v} = -\eta_2 e_{z_v} \quad (49)$$

$$\dot{z_v} - \dot{z_v{}^d} = -\eta_2(z_v - z_v{}^d) \quad with\ \eta_2 > 0$$

This gives

$$-\frac{1}{\tau}z_v + \frac{1}{\tau}u - \dot{z_v{}^d} = -\eta_2(z_v - z_v{}^d) \quad (50)$$

From which the following expression for the physical input u is deduced:

$$u = \frac{\frac{1}{\tau}z_v + \dot{z}_v^d - \eta_2(z_v - z_v{}^d)}{1/\tau} \quad (51)$$

By applying the above design, the closed loop system will be asymptotically stable with control Lyapunov function $V(z) = \frac{1}{2}e_A{}^2 + \frac{1}{2}e_{z_v}{}^2$, where $\eta_2 > \eta_1 > 0$, which control the speed of convergence.

b. High level controller (Chassis Supervisor)

The main objective of the control of the active suspension is to reduce the effect of irregularities of the road to improve the passenger's comfort and to increase safety during critical maneuvers, by roll and roll rate compensation. For this purpose a backstepping method is proposed.

First, the control function u_z for the heave motion is designed to guarantee the convergence of the tracking error $e_{z1} = z - z_{ref}$ to zero. Starting with the equation of tracking error $e_{z1} = z - z_{ref}$, we have $\dot{e}_{z1} = \dot{z} - \dot{z}_{ref}$.

Choose a virtual control $\dot{z}^d$ to make the tracking error e_{z1} converges to zero. Let $e_{z2} = \dot{z} - \dot{z}^d$, then:

$$\dot{e}_{z1} = (e_{z2} + \dot{z}^d) - \dot{z}_{ref} \quad (52)$$

Considering a Lyapunov function candidate as follows:

$$V_1 = \frac{1}{2}e_{z1}^2 \quad (53)$$

The time derivative of V_1 :

$$\dot{V}_1 = e_{z1} * \dot{e}_{z1} \quad (54)$$

$$= e_{z1} * (e_{z2} + \dot{z}^d - \dot{z}_{ref})$$
$$= e_{z1} * e_{z2} + e_{z1}(\dot{z}^d - \dot{z}_{ref})$$

Choose

$$(\dot{z}^d - \dot{z}_{ref}) = -\eta_{z1} * \tanh(e_{z1}) \quad (55)$$

$$\dot{V}_1 = e_{z1} * e_{z2} - e_{z1} * \eta_{z1} * \tanh(e_{z1}) \quad (56)$$

Clearly, if e_{z2}=0, then $\dot{V}_1 = -\eta_{z1}e_1 tanh(e_{z1}) \leq 0$ and e_{z1} is guaranteed to converge to zero asymptotically [31].

Then synthesize a control law for u_Z, so that the error e_{z2} converges to zero. Differentiating the error dynamics e_{z2} results in:

$$\dot{e}_{z2} = \ddot{z} - \ddot{z}^d = f_z(x,\dot{x}) + g_z(x,\dot{x}) * u_Z - \ddot{z}_{ref} + \eta_{z1}(1 - tanh^2(e_{z1}))\dot{e}_{z1} \quad (57)$$

Choosing the control law as following:

$$u_Z = g_z(x,\dot{x})^{-1}(-\eta_{z1}(1 - tanh^2(e_{z1}))\dot{e}_{z1} + \ddot{z}_{ref} - \eta_{z2}tanh(e_{z2}) - e_{z1} - f_z(x,\dot{x})) \quad (58)$$

Then,

$$\dot{e}_{z2} = -\eta_{z2}tanh(e_{z2}) - e_{z1} \quad (59)$$

$$where\ \eta_{z2} > 0$$

And choosing a Lyapunov function candidate:

$$V_2 = V_1 + \frac{1}{2}e_{z2}^2 \quad (60)$$

Calculating its time derivative gives:

$$\dot{V}_2 = \dot{V}_1 + e_{z2} * \dot{e}_{z2} = e_{z1} * e_{z2} - e_{z1}\eta_{z1}\tanh(e_{z1}) + e_{z2}(-\eta_{z2}\tanh(e_{z2}) - e_{z1}) = -e_{z1}\eta_{z1}\tanh(e_{z1}) - e_{z2}\eta_{z2}\tanh(e_{z2}) \leq 0 \quad (61)$$

Following a similar procedure, the resultant control function $u_\theta\ and\ u_\phi$ for pitch and roll motion can be obtained as:

$$u_\theta = g_\theta(x,\dot{x})^{-1}(-\eta_{\theta1}(1 - tanh^2(e_{\theta1}))\dot{e}_{z1} + \ddot{\theta}_{ref} - \eta_{\theta2}tanh(e_{\theta2}) - e_{\theta1} - f_\theta(x,\dot{x})) \quad (62)$$

$$u_\phi = g_\phi(x,\dot{x})^{-1}(-\eta_{\phi1}(1 - tanh^2(e_{\phi1}))\dot{e}_{\phi1} + \ddot{\phi}_{ref} - \eta_{\phi2}tanh(e_{\phi2}) - e_{\phi1} - f_\phi(x,\dot{x})) \quad (63)$$

In order to obtain the desired forces $f_{fr}{}^d, f_{rr}{}^d, f_{fl}{}^d, f_{rl}{}^d$, we use the relation between the control inputs computed and the forces (6) that is:

$$\begin{pmatrix} u_z \\ u_\theta \\ u_\phi \end{pmatrix} = \begin{pmatrix} 1 & 1 & 1 & 1 \\ a & a & -b & -b \\ -w & w & -w & w \end{pmatrix} \begin{pmatrix} {f_{fr}}^d \\ {f_{fl}}^d \\ {f_{rr}}^d \\ {f_{rl}}^d \end{pmatrix} \quad (64)$$

A fourth relation added to the three above relations: the Roll Stiffness Distribution (RSD) factor $\alpha_{RSD}(t)$[32]. RSD factor distributes the active roll moments to the front and rear suspensions in way that causes variable load transfer distribution and influence tire side force saturation properties in the front and rear axles respectively and thus the lateral and longitudinal stability.

The relation is as follows:

$$w\left({f_{fl}}^d - {f_{fr}}^d\right) = \alpha_{RSD}(t) * u_\phi \quad (65)$$

Then calculating the desired forces as follows:

$$f^d = \begin{pmatrix} {f_{fr}}^d \\ {f_{fl}}^d \\ {f_{rr}}^d \\ {f_{rl}}^d \end{pmatrix} = \begin{pmatrix} 1 & 1 & 1 & 1 \\ a & a & -b & -b \\ -w & w & -w & w \\ -w & w & 0 & 0 \end{pmatrix}^{-1} \begin{pmatrix} u_z \\ u_\theta \\ u_\phi \\ \alpha_{RSD}(t) * u_\phi \end{pmatrix} \quad (66)$$

VI. Control Strategy

In order to obtain a global chassis control, a coordinated control strategy between the three subsystems; active steering, differential braking and active suspension was implemented. Active steering and differential braking plays an important role in stabilizing the lateral dynamics of the vehicle. In addition, active suspension system shows its good effect on lateral stability during maneuvering, using a proposed strategy for the distribution of its active forces f_ϑ. This strategy also shows its efficiency in decreasing the propensity of rollover accidents in critical maneuvers at the same time by providing an anti-roll moment that decreases the roll angle and roll rate by the active suspension system. In normal driving situations, it provides comfort to passengers and road holding.

Indeed, in normal driving situations (*safe region*), the lateral acceleration and roll angle have small values. In this case, the active suspension system work in the trade off choice to improve comfort and road holding by converging $z, \theta \; and \; \phi$ to their reference values, which are chosen to be zero in our study to achieve our objectives . We name this case as "*soft-case*". When the driving situation reaches the dangerous region, the vehicle stability is weak, lateral acceleration a_y increases and the propensity for rollover increases (*critical region*). In this situation, the priority is given to roll angle and roll rate compensation, so a smooth switching to higher values is applied to the control parameters of active suspension controller, and this case is named as "*hard-case*".
The switching operation is implemented with the help of widely used index in the literature, which is the *SSF index* [33]. It represents the Static Stability Factor equal to $\frac{a_y}{g}$, it helps us to indicate the transition threshold between safe and critical region. Fig. 5 shows the switching operation for the control parameters corresponding to the backstepping method discussed before (V.C.). In safe region the parameters $(\eta_{z1}, \eta_{\theta 1} \; and \; \eta_{\phi 1})$ have the small value $\eta_1^s \; and \; \eta_2^s$ and in critical region the values will increase smoothly to reach the values $\eta_1^h \; and \; \eta_2^h$. In this way, the roll compensation and anti-roll moment increases.

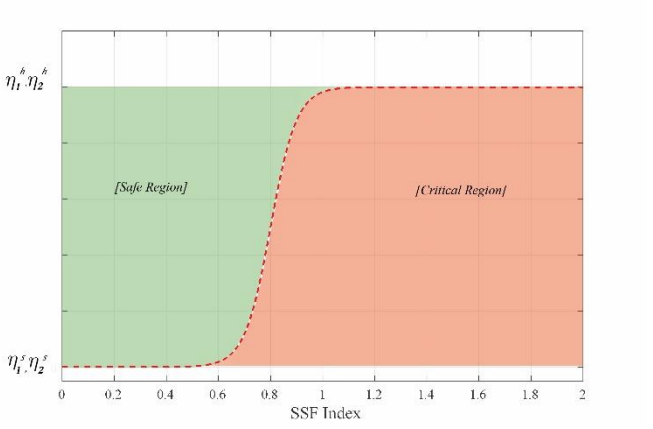

Figure 5. Control Strategy (1).

By providing anti-roll moment, the controller shows its effectiveness in decreasing the rollover propensity. However, after simulating several test maneuvers, it is recognized that reducing the body roll angle causes the vehicle to slide laterally rather than to roll over. Therefore, it is important to implement a complementary strategy for the distribution of vertical suspension forces in a way that gives the lateral or longitudinal forces that create a convenient moment around the z-axis to stabilize the lateral vehicle dynamics. A proposed solution to increase stability is illustrated in Fig. 6.

Fig. 6 shows the variation in the distribution of the desired forces, calculated by the higher-level controller that aims to converge $z, \theta, and \; \phi$ to their references $z_{ref}, \theta_{ref} \; and \; \phi_{ref}$, as function of *SI*. The *Stability Index (SI),* introduced in [13], calculates the vehicle's lateral stability region out of the phase plane of the side-slip angle and its time derivative as:

$$SI = |2.49\beta + 9.55\dot{\beta}| \quad (67)$$

Where $SI < 1$ corresponds to the stable region for $\mu = 1$ (coefficient of adherence). For $SI < 1$, the value of α_{RSD} is chosen to be equal to 0.5, so that does not affect the distribution of forces results from the first three relations in (64). When the vehicle lateral dynamics enter in unstable region, $SI > 1$, the value of α_{RSD} will change (Fig.6) . The basis of using this strategy is that the behavior of the vehicle at the limits of adhesion is quite different from its nominal behavior. At the limits of adhesion, the slip angle is high and the sensitivity of yaw moment to changes in steering angle becomes highly reduced. At large slip angles, changing the steering angle produces very little change in the yaw rate of the vehicle. This strategy addresses these issues by reducing the deviation of the vehicle behavior from its normal behavior on dry roads and by preventing the vehicle slip angle from becoming large.[26]

Since the total amount of grip available in tires is not fixed, it is in fact depends in fact on a number of factors, one of which is the amount of

weight acting on the wheel. If you decrease the amount of weight acting on the contact patch, this artificially lowers the amount of adhesion available, and vice versa. So two cases are studied, if $|\dot{\psi}_{ref}| > |\dot{\psi}|$, the vehicle has more tendency to be in understeer situation, then the available grip in front wheels is exceeded, so a forward weight transfer is applied so that it increase the adhesion in the front wheels which free up more grip to steer. For this purpose a smooth switching for the value of α_{RSD} from 0.5 to higher values is

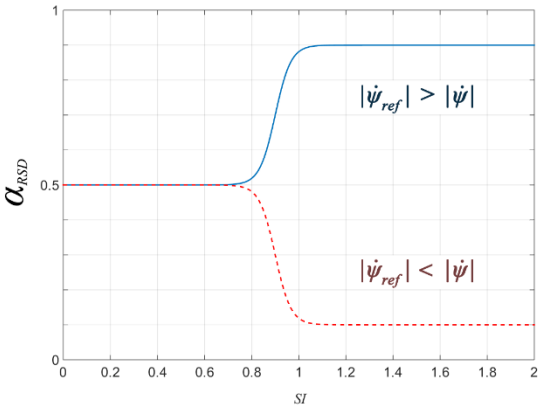

Figure 6. Control strategy (2).

applied (e.g. 0.9). If $|\dot{\psi}_{ref}| < |\dot{\psi}|$, the vehicle has more tendency to be in oversteer situation, then the available grip in rear wheels is exceeded, so a backward weight transfer is applied so that it increase the adhesion in the rear wheels which free up more grip to correct the loss of traction and reduce vehicle rotation. For this purpose, a smooth switching for the value of α_{RSD} from 0.5 to lower values is applied (e.g. 0.1).

In some critical driving situations, the active suspension system is not sufficient and it is difficult for the driver to stabilize the vehicle. Safety of ground vehicles requires the improvement of yaw stability by active controller. In the stability region, only the AFS controller must be involved in the vehicle's control by tracking the yaw rate error to zero. The brake-based DYC, which tracks down the side-slip angle error to zero, is not recommended in normal driving situations since it decelerates the vehicle. Therefore, it will be activated only when the vehicle goes toward the instability region to assist the AFS controller. On the other hand and since the AFS will have no effect outside the vehicle stability region, the AFS controller will be deactivated when the vehicle goes toward the instability region.

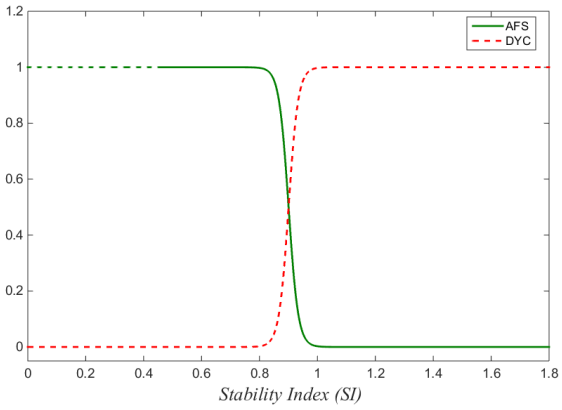

Figure 7. Control strategy (3).

This coordination between AFS and the differential braking is illustrated in Fig.7, where "1" means activated and "0" means deactivated. The coordination block is implemented between the controllers, and in order to prevent sudden changes in the system dynamics a smooth transition should be ensured while the controllers pass from active to inactive state and vice versa.

The scheme of Fig. 8 shows the general structure for the whole control system:

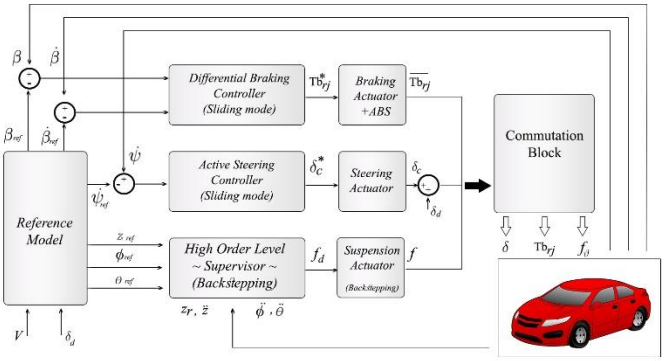

Figure 8. General structure of Global Chassis control system.

VII. Test Maneuvers

To demonstrate the effect of the designed control strategy, two simulations are conducted on the full vehicle model, both are critical driving situations widely used for testing controllers, one for stability and the other for rollover.

In this section, in addition to SSF and SI index, we will use another two indexes that are a vehicle rollover threat index.

a) *LTR* index, the vehicle load transfer ratio (LTR) is defined by:

$$LTR = \frac{Load\ on\ Right\ Tires\ -\ Load\ on\ Left\ Tires}{Total\ Load}$$

Clearly, LTR varies within [−1, 1], and it is equal to zero for a symmetric car that is driving straight. The bounds LTR ∈ {−1, 1} are reached in the case of a wheel lift-off on either side of the vehicle. This indication capability of the LTR is useful in design of rollover prevention schemes. A dynamical approximation for the load transfer ratio, denoted LTR_d [34], is given as follows where c_ϕ *and* k_ϕ are damping and roll stiffness respectively.

$$LTRd = \frac{-2(c_\phi \dot{\phi} + k_\phi \phi)}{mgT} \qquad (68)$$

b) *RI index*

The RI is a dimensionless number that can indicate a danger of vehicle rollover. The RI is calculated by using the measured lateral acceleration, the roll angle, and the roll rate, and their critical values depend on vehicle geometry as follows [35]:

$$RI = \begin{cases} \omega_1\left(\frac{|\phi(t)|\dot{\phi}_{th}+|\dot{\phi}(t)|\phi_{th}}{\dot{\phi}_{th}\phi_{th}}\right)+\omega_2\left(\frac{|a_y|}{a_{y,c}}\right) \\ \quad +(1-\omega_1-\omega_2)\left(\frac{|\phi(t)|}{\sqrt{(\phi(t))^2+(\dot{\phi}(t))^2}}\right), & \phi(\dot{\phi}-\ell\phi)>0 \\ 0 \qquad\qquad\qquad\qquad\qquad\qquad , & \phi(\dot{\phi}-\ell\phi)\le 0 \end{cases} \tag{69}$$

Where $\omega_1, \omega_2,$ and ℓ are positive constants. $\dot{\phi}_{th}, \phi_{th}$ and $a_{y,c}$ are chosen to be $50\ deg/s$, $7\ deg, and\ 8\ m/s^2$ respectively [36].

A. Double-lane-change (DLC) maneuver on a dry road at 120 km/h:

In the first simulation, the vehicle negotiates a double-lane-change maneuver on a dry road ($\mu = 0.95$). This maneuver is often used in the vehicle handling performance test. We choose an initial speed of 120 *km/h,* and a peak steering wheel angle of magnitude of $\delta_{d,max} = 5°$. The steering profile corresponding to this maneuver is shown in Fig. 9.

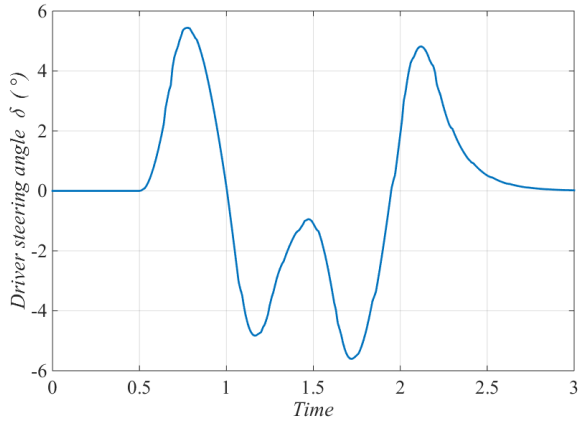

Figure 9. Driver steering input angle.

First, to demonstrate the effectiveness of the second control strategy (Fig. 6), a comparison is done between the performance of the passive system, the system with AS without second strategy, and the system with AS and second strategy (αAS). Fig.10 shows the active suspension forces introduced to the vehicle with second strategy (blue) and without it (red). Fig. 11-14 show how did the active suspension system with the second strategy enhance vehicle stability.

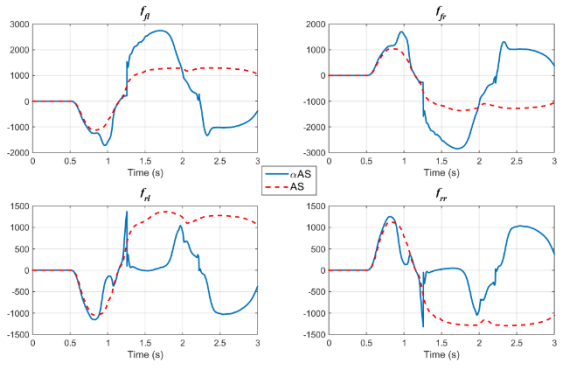

Figure 10. Active suspension forces.

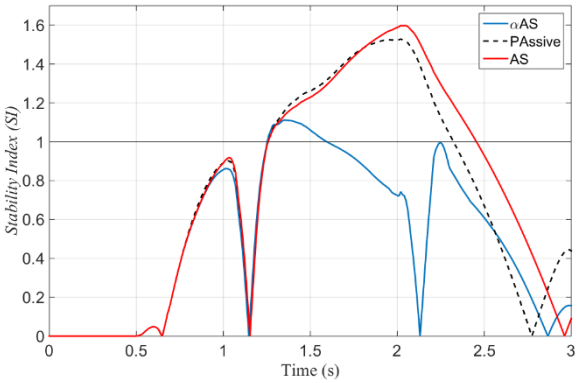

Figure 11. Comparison of Stability index between AS and αAS.

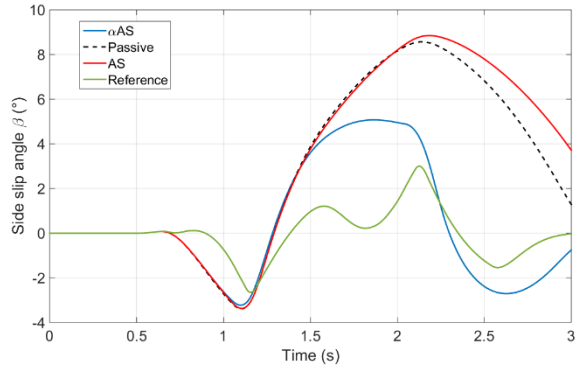

Figure 12. Comparison of sideslip angle between αAS and AS.

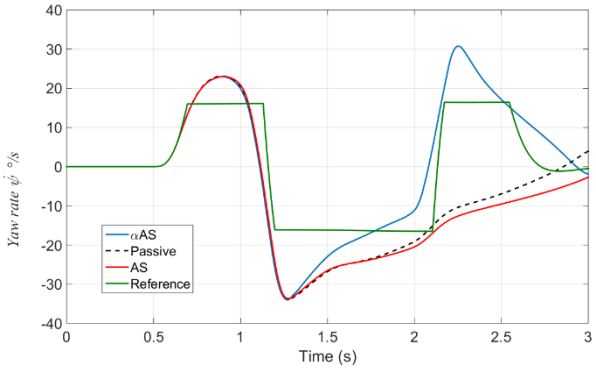

Figure 13. Comparison of Yaw rate between αAS and AS.

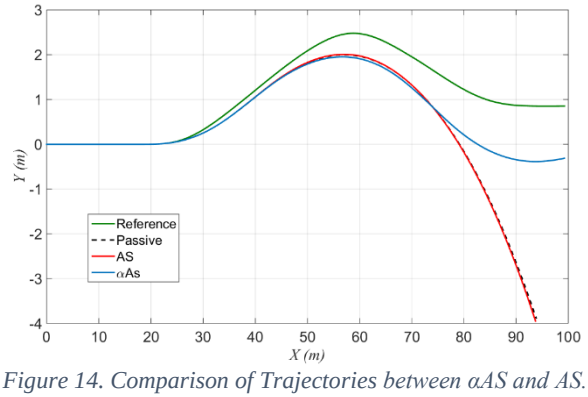

Figure 14. Comparison of Trajectories between αAS and AS.

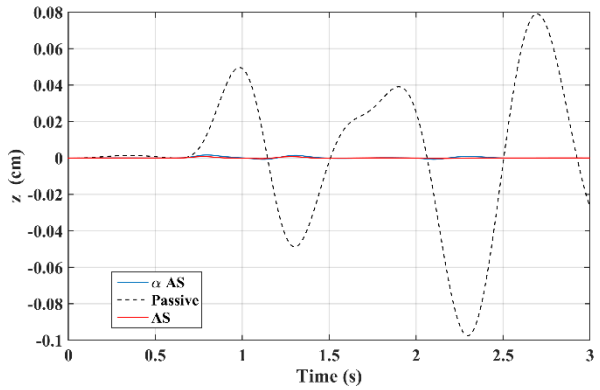

Figure 15. Z CoG displacement.

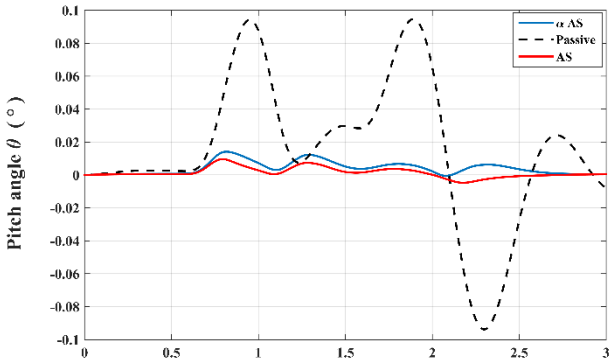

Figure 16. Pitch angel θ (°).

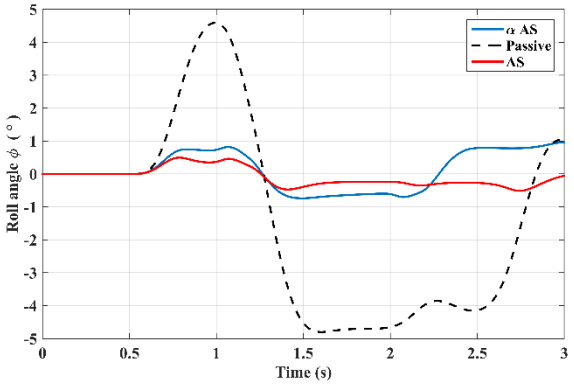

Figure 17. Roll angel ϕ (°).

It is obvious in Fig. 11 that the value of *SI* gets smaller with the system with the second strategy. The sideslip angle is lower (Fig.12) and the sensitivity of yaw rate to the changes in steering angle increased as shown in Fig.13. In Fig.14, it is clearly shown how the forward weight transfer can reduce understeer and improve maneuverability. Fig. 15-17, represent the comparison done for the displacement of the center of gravity, the pitch and roll dynamics. It is seen that the second strategy has small acceptable effect on the vertical dynamic of the vehicle as well as the pitch angle and roll angle.

But, it is deduced that adding the active suspension system to the vehicle maybe not sufficient to provide a safe driving through a critical maneuvering. Therefore, we add the two other active systems, the active steering and differential braking system. Fig.18-19 represent the output of the three active actuators as function of time.

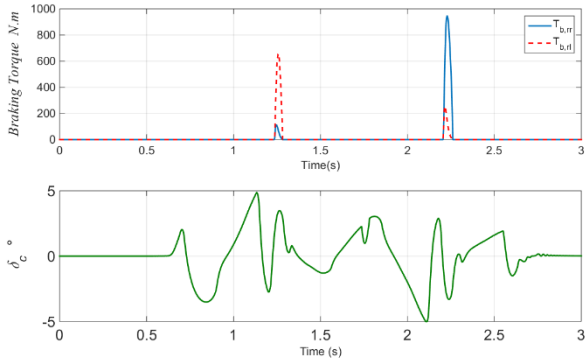

Figure 18. Differential braking and active steering control output.

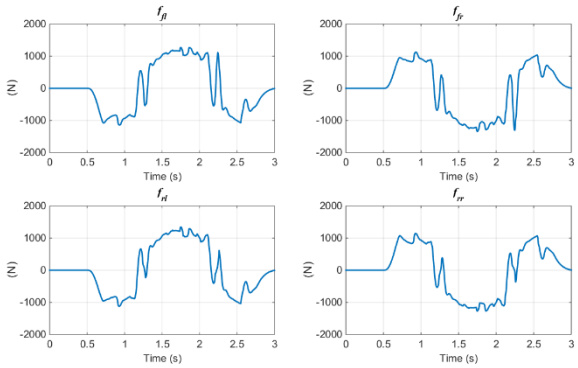

Figure 19. Active suspension forces (αAS).

Fig. 20 - 26 compare the fully coordinated controlled system, the passive system and the generated reference model. Fig. 20 shows in blue how did the full controlled vehicle operates in the safe region (SI<1) during the maneuver where the SI_{peak}=0.9.

Fig. 21 represents the yaw rate response versus time. It shows that the uncontrolled vehicle significantly lags the desired yaw rate, while the controlled vehicle closely tracks the reference response. A comparison between the sideslip angles of the controlled and uncontrolled vehicles is illustrated in Fig. 22. The vehicle with integrated control achieves lower peaks values for sideslip angle compared to the passive system. Then an improvement in handling performance is obtained with the proposed controller. Fig. 23 shows the longitudinal and lateral velocities, it is noticed that the passive system decelerated more than the controlled one, and the lateral speed had smaller values in controlled system rather than the passive vehicle which indicates a better performance for the controlled vehicle.

Although the controlled vehicle improves stability, it compensates the body roll angle and roll rate at the same time, and that what appears obviously in Fig. 24. Which then leads to the lower values for both rollover indexes as shown in Fig. 25. Finally yet importantly, in Fig. 26, the trajectories of the controlled and passive vehicles are compared to the ideal trajectory. It can be noticed that the controlled vehicle tracks

better the desired path, where the passive vehicle went out the desired trajectory.

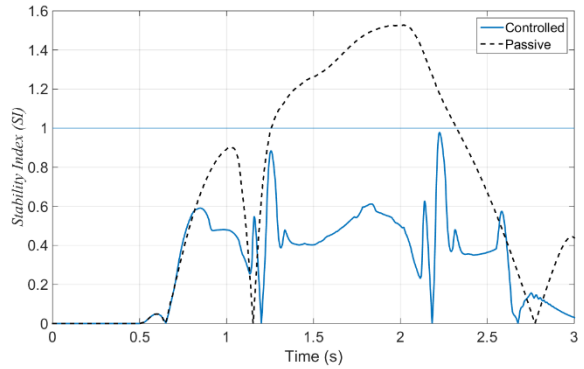

Figure 20. Stability index (SI), DLC.

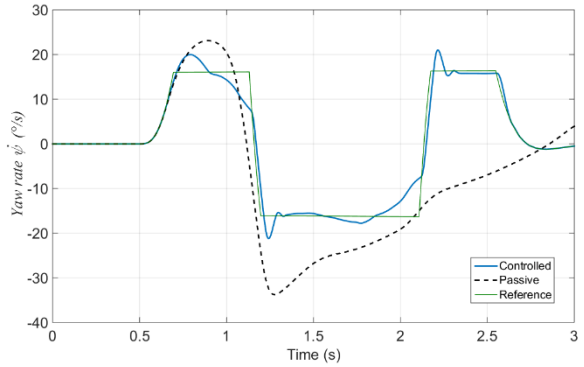

Figure 21. Yaw rate $\dot{\psi}$.

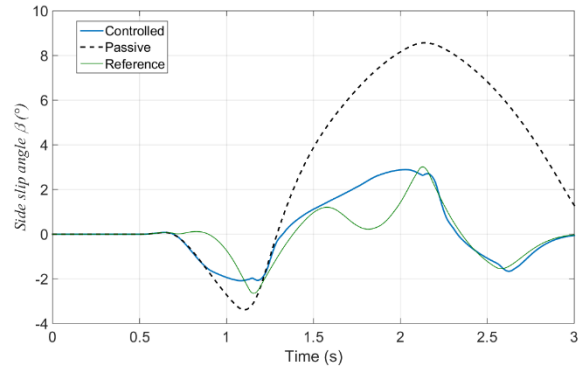

Figure 22. Sideslip angle β (°).

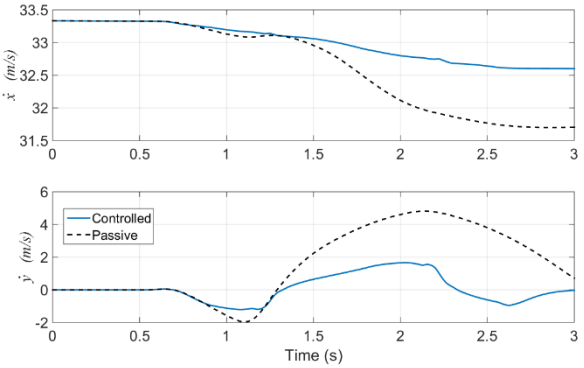

Figure 23. Longitudinal and lateral velocities.

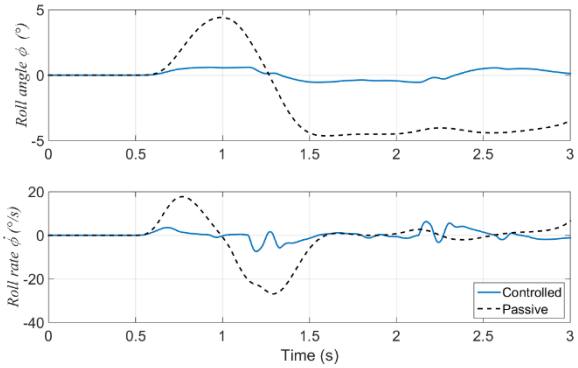

Figure 24. Roll angle and roll rate.

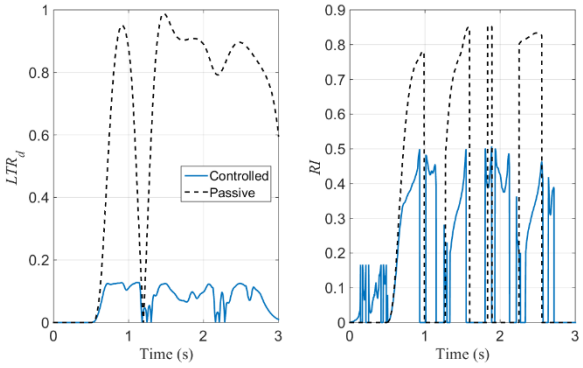

Figure 25. LTR_d and RI.

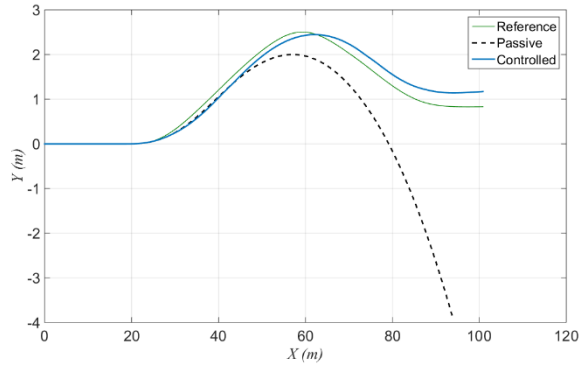

Figure 26. Vehicle trajectories.

B. J-turn maneuver on a dry road at 65km/h.

In the second simulation, the vehicle negotiates a J-turn maneuver on a dry road. This maneuver is often used in the vehicle rollover test. The goal of this test is to show the

effectiveness of the controller in decreasing rollover propensity. Fig. 27 introduces the driver steering profile.

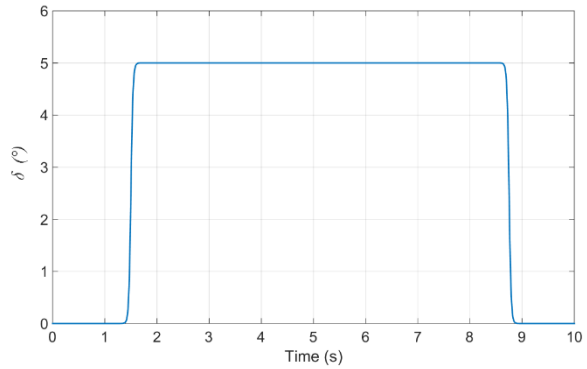

Figure 27. J-turn Driver steering input.

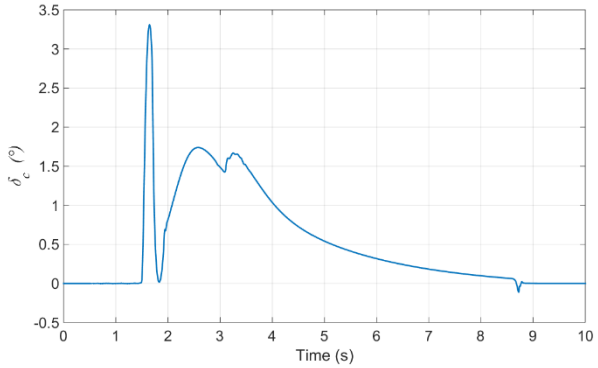

Figure 28. Active steering output.

Fig. 28 shows the output of the active steering actuator that regulates the yaw rate and makes it track it's reference. Fig. 29 shows the braking torques applied on the rear wheels during maneuver. This braking torques reduce the vehicle longitudinal speed that has a direct effect on the lateral acceleration according to (12).

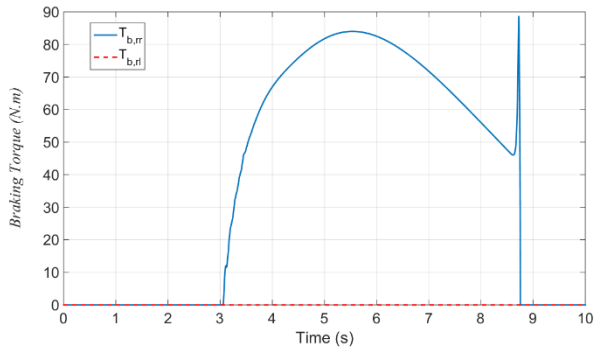

Figure 29. Braking Torque (N.m).

Decreasing a_y plays a crucial role in reducing rollover propensity, but may be not sufficient. Here the active suspension system forces (Fig. 30) assist in providing an anti-roll moment along the roll axis that decreases roll angle and roll rate. In Fig. 31 - 32, we can see the compensation in roll angle and roll rate that has the most effects on preventing rollover accidents. Moreover, reduction in suspension stroke provides more handling and road holding for the driver. Fig. 33 shows the reduction on the variation of suspension stroke.

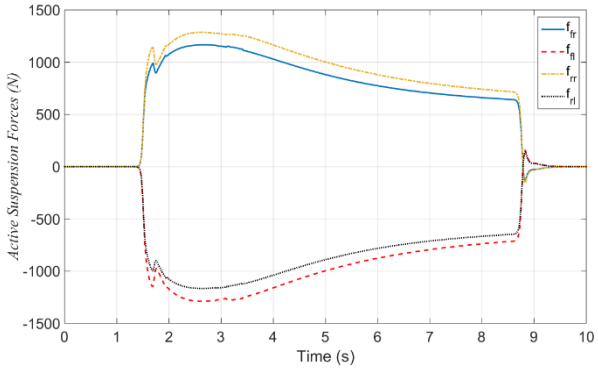

Figure 30. Active suspension forces.

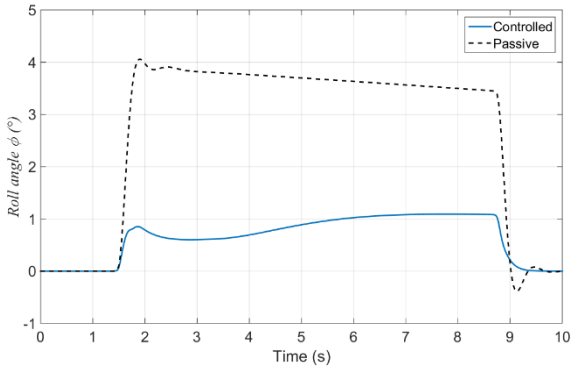

Figure 31. Roll angle .

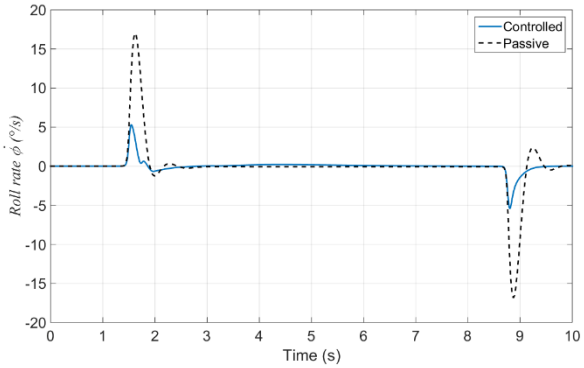

Figure 32. Roll rate $\dot{\phi}$.

The results in Fig. 34 show that the uncontrolled system gets nearer to the critical limits, the rollover indexes indicate impending vehicle rollover, but the controlled system stays in the safe region where RI_{max}=0.55, and LTR_{max}=0.25. This means that the vehicle with coordinated strategy controller proves its effectiveness in decreasing rollover danger.

It can be observed in Fig. 35, that the controlled vehicle tracks better the desired path, where the passive vehicle went out the desired trajectory with a high probability to rollover the road. Fig. 36 shows the stability index value and Fig. 37 shows the how the controlled system tracks the reference of the yaw rate perfectly.

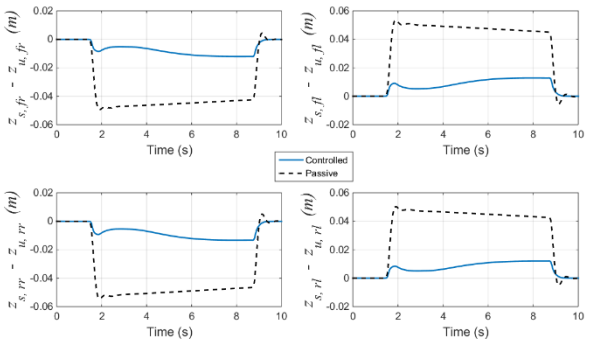

Figure 33. Suspension stroke $z_{s,v} - z_{u,v}$.

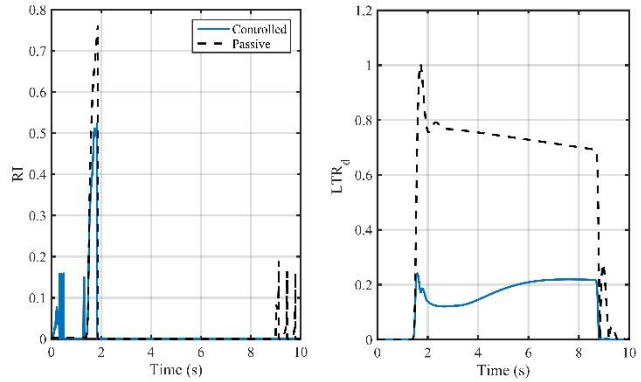

Figure 34. LTR_d and RI indexes.

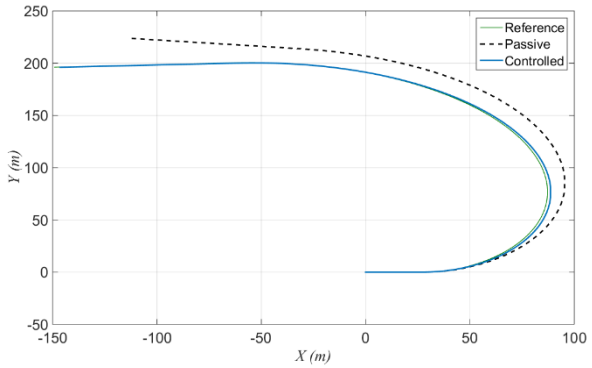

Figure 35. Vehicle Trajectories.

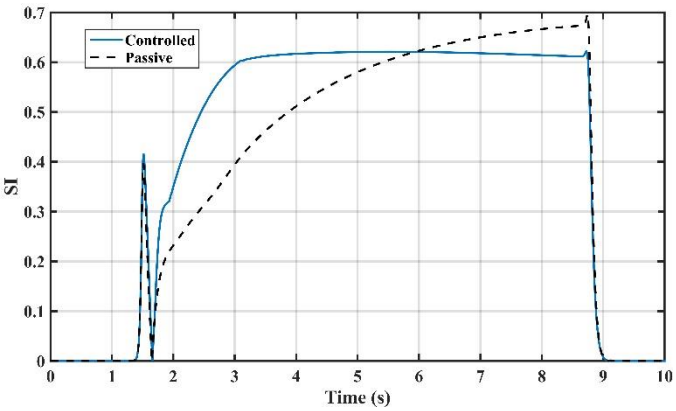

Figure 36. . Stability index (SI), J-turn.

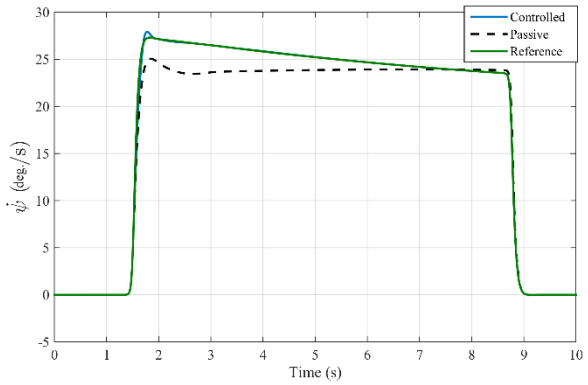

Figure 37. . Yaw rate $\dot{\psi}$

VIII. CONCLUSION

In this paper, a Global Chassis Control has been proposed, based on a coordination control strategy between active suspension, active front steering and differential braking systems. It aims to ensure stability and rollover prevention on road vehicles. Nonlinear adaptive and robust control technics have been developed to control the active actuators, as the backstepping and the second order sliding mode control. The performance of the proposed control strategy in achieving safety has been validated in simulation on a full vehicle model, under several scenarios. Two types of maneuvers have been used: first, a double lane change maneuver where we have to prevent vehicle skidding, second, a J-turn maneuver where a rollover or near-rollover incident must be avoided. Simulation results emphasize the success of the collaborative strategy for enhancing lateral and vertical dynamics, and have shown the efficiency of the proposed approach. It has been verified that the proposed control coordination shows good performance in rollover prevention and achieving good vehicle lateral stability. The perspective of our work will be concentrated to find the correlation between the distribution of the active suspension forces and the anti-moment produced around the z-axis to reach more stabilizing vehicle in most critical maneuvers. In that way we can achieve, using active suspension system, a comfort driving for passenger and road holding in normal driving situations, and vehicle stability and rollover prevention in critical situations.

ACKNOWLEDGMENT

This work was supported by the French Lebanese Research program CEDRE (32918PA).

REFERENCES

[1] A. Chamseddine, T. Raharijaona, and H. Noura, "Sliding Mode Control Applied to Active Suspension Using Nonlinear Full Vehicle and Actuator Dynamics," *Proc. 45th IEEE Conf. Decis. Control*, pp. 3597–3602, 2006.

[2] N. Yagiz and Y. Hacioglu, "Backstepping control of a vehicle with active suspensions," *Control Eng. Pract.*, vol. 16, no. 12, pp. 1457–1467, 2008.

[3] M. Q. Nguyen, O. Sename, and L. Dugard, "A

motion-scheduled LPV control of full car vertical dynamics," *2015 Eur. Control Conf. ECC 2015*, pp. 129–134, 2015.

[4] X. Shao, N. Zhang, H. Du, and L. Wang, "Fuzzy control of hydraulically interconnected suspension with configuration switching," *Proc. 2013 IEEE Int. Conf. Veh. Electron. Safety, ICVES 2013*, no. 51175157, pp. 66–71, 2013.

[5] G. D. Nusantoro and G. Priyandoko, "PID State Feedback Controller of a Quarter Car Active Suspension System," vol. 1, no. 11, pp. 2304–2309, 2011.

[6] S. Mouleeswaran, "Design and Development of PID Controller-Based Active Suspension System for Automobiles," *PID Controll. Des. Approaches-Theory, Tuning, Appl. to Front. Areas*, vol. II, pp. 71–98, 2012.

[7] L. Wang, N. Zhang, and H. Du, "Design and experimental investigation of demand dependent active suspension for vehicle rollover control," *Proc. IEEE Conf. Decis. Control*, pp. 5158–5163, 2009.

[8] S. Yim, "Design of a robust controller for rollover prevention with active suspension and differential braking," *J. Mech. Sci. Technol.*, vol. 26, no. 1, pp. 213–222, 2012.

[9] N. C. Parida, S. Raha, and A. Ramani, "Rollover-preventive force synthesis at active suspensions in a vehicle performing a severe maneuver with wheels lifted off," *IEEE Trans. Intell. Transp. Syst.*, vol. 15, no. 6, pp. 2583–2594, 2014.

[10] C. Bardawil, R. Talj, C. Francis, A. Charara, and M. Doumiati, "Integrated Control for Vehicle Lateral Dynamics Improvements using Second Order Sliding Mode," *IEEE Conf. Control Appl.*, pp. 322–327, 2014.

[11] M. Doumiati *et al.*, "Vehicle yaw control via coordinated use of steering/braking systems," *IFAC Proc. Vol.*, vol. 44, no. 1, pp. 644–649, 2011.

[12] D. a C. Junjie He Martin C. Levesley and W. J. Manning, "Integrated Active Steering and Variable Torque Distribution Control for Improving Vehicle Handling and Stability," *Proc. 2004 SAE World Congr.*, vol. 2004, no. 724, p. 12, 2004.

[13] J. He, "Integrated Vehicle Dynamics Control using Active Steering, Driveline and Braking," The University of Leeds School of Mechanical Engineering, 2005.

[14] M. Doumiati *et al.*, *Vehicle yaw control via coordinated use of steering/braking systems*, vol. 18, no. PART 1. IFAC, 2011.

[15] R. Rajamani, *Vehicle Dynamics and Control*. New York, NY,: Springer US, 2006.

[16] A. Hac, "Rollover stability index including effects of suspension design," *Sae Tech. Pap. 2002-01-0965*, vol. SP–1656, no. 724, pp. 68–78, 2002.

[17] U. Kiencke and L. Nielsen, *Automotive control systems U. Kiencke and L. Nielsen; Springer, Berlin, 2000, ISBN-3-540-66922-1*, vol. 38, no. 6. 2002.

[18] W. F. Milliken and D. L. Milliken, *Race Car Vehcile Dynamics*, vol. 53, no. 9. 2013.

[19] R. P. Osborn and T. Shim, "Independent control of all-wheel-drive torque distribution," *Veh. Syst. Dyn.*, vol. 44, no. 7, pp. 529–546, 2006.

[20] H. Shraim, M. Ouladsine, and L. Fridman, "Sliding mode observers to replace vehicles expensive sensors and to preview driving critical situations," *Int. J. Veh. Auton. Syst.*, vol. 5, no. 3, pp. 345–361, 2007.

[21] M. Doumiati, A. Charara, A. Victorino, and D. Lechner, *Vehicle Dynamics Estimation using Kalman Filtering: Experimental Validation*. Wiley, 2012.

[22] T. a. Wenzel, K. J. Burnham, M. V. Blundell, and R. a. Williams, "Dual extended Kalman filter for vehicle state and parameter estimation," *Veh. Syst. Dyn. Int. J. Veh. Mech. Mobil.*, vol. 44, no. 2, pp. 153–171, 2006.

[23] H. Shraim, M. Ouladsine, M. El Adel, and H. Noura, "A new analytical model representation for vehicle dynamics in the plan (X, Y)," *IFAC Proc. Vol.*, vol. 38, no. 1, pp. 230–235, 2005.

[24] H. Dugoff, P. S. Fancher, and L. Segel, "An Analysis of Tire Traction Properties and Their Influence on Vehicle Dynamic Performance," *SAE Pap. 700377*, pp. 1219–1243, 1970.

[25] J. Ackermann and T. Bünte, "Yaw disturbance attenuation by robust decoupling of car steering," *Control Eng. Pract.*, vol. 5, no. 8, pp. 1131–1136, 1997.

[26] R. Rajamani, *Vehicle Dynamics and Control*, 2nd ed. New York, NY,: Springer US, 2012. pp. 202–213.

[27] R. Sartori, S. M. Savaresi, and M. Tanelli, "Combining slip and deceleration control for brake-by-wire control systems: A Sliding-mode Approach," European Journal of Control, 2007, pp. 593–611.

[28] Y. Shtessel, C. Edwards, L. Fridman, and A. Levant, *Sliding Mode Control and Observation*. Springer New York, 2014.

[29] A. Levant, "Sliding order and sliding accuracy in sliding mode control," *Int. J. Control*, vol. 58, no. 6, pp. 1247–1263, 1993.

[30] S. Anwar, "Yaw stability control of an automotive vehicle via generalized predictive algorithm," *Proc. 2005, Am. Control Conf. 2005.*, pp. 435–440, 2005.

[31] W. Sun, H. Gao, and O. Kaynak, "Adaptive Backstepping Control for Active Suspension Systems With Hard Constraints," *IEEE/ASME Trans. Mechatronics*, vol. 18, no. 3, pp. 1–8, 2012.

[32] X. Moreau, A. Rizzo, A. Oustaloup, and D. Libération, "Application of the CRONE control-design method to a low-frequency active suspension system," *Int. J. Veh. Auton. Syst.*, vol. 7, no. 3–4, pp. 172–200, 2009.

[33] NHTSA, TRB, and N. R. C. (U. S.). C. for the Study of a Motor Vehicle Rollover Rating System, "The National Highway Traffic Safety Administration's Rating System for Rollover Resistance: An Assessment," Transportation Research Board, 2002.

[34] S. Solmaz, M. Corless, and R. Shorten, "A methodology for the design of robust rollover prevention controllers for automotive vehicles: Part 2-Active steering," *Proc. Am. Control Conf.*, no. 1, pp. 1606–1611, 2007.

[35] J. Yoon, D. Kim, and K. Yi, "Design of a rollover

index-based vehicle stability control scheme," *Veh. Syst. Dyn.*, vol. 45, no. July 2015, pp. 459–475, 2007.

[36] J. Kang, J. Yoo, and K. Yi, "Driving control algorithm for maneuverability, lateral stability, and rollover prevention of 4WD electric vehicles with independently driven front and rear wheels," *IEEE Trans. Veh. Technol.*, vol. 60, no. 7, pp. 2987–3001, 2011.